

# Pointmap-Conditioned Diffusion for Consistent Novel View Synthesis

Thang-Anh-Quan Nguyen<sup>1,2</sup>, Nathan Piasco<sup>1</sup>, Luis Roldão<sup>1</sup>, Moussab Bennehar<sup>1</sup>,  
Dzmitry Tsishkou<sup>1</sup>, Laurent Caraffa<sup>3</sup>, Jean-Philippe Tarel<sup>2</sup>, Roland Brémond<sup>2</sup>

<sup>1</sup>Noah’s Ark, Huawei Paris Research Center, France

<sup>2</sup>COSYS, Gustave Eiffel University, France

<sup>3</sup>LASTIG, Gustave Eiffel University, IGN-ENSG, France

## Abstract

In this paper, we present *PointmapDiffusion*, a novel framework for single-image novel view synthesis (NVS) that utilizes pre-trained 2D diffusion models. Our method is the first to leverage pointmaps (i.e. rasterized 3D scene coordinates) as a conditioning signal, capturing geometric prior from the reference images to guide the diffusion process. By embedding reference attention blocks and a ControlNet for pointmap features, our model balances between generative capability and geometric consistency, enabling accurate view synthesis across varying viewpoints. Extensive experiments on diverse real-world datasets demonstrate that *PointmapDiffusion* achieves high-quality, multi-view consistent results with significantly fewer trainable parameters compared to other baselines for single-image NVS tasks.

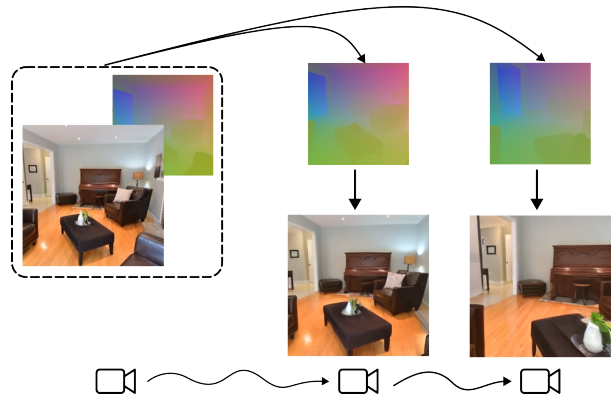


Figure 1. Starting from a single input image, PointmapDiffusion generates coherent novel views and ensures visual consistency and realism along a chosen camera path.

## 1. Introduction

Novel View Synthesis is a core problem in computer vision and graphics. It aims to synthesize high-quality, realistic images of a scene from unseen viewpoints, which can enhance user immersion in applications such as virtual reality (VR) and augmented reality (AR). Existing approaches for novel view synthesis, such as those in [8, 27, 28], often rely on extensive multi-view datasets and require optimizing a 3D representation to generate realistic results. In contrast, our method targets single-shot view synthesis using a diffusion-based framework [14]. Unlike multi-view synthesis, where multiple perspectives aid in reconstructing scenes, single-shot view synthesis poses unique challenges as it must generate plausible unseen areas without additional views while retaining consistency, making the task inherently ambiguous.

Many state-of-the-art methods focus on generative-based NVS by leveraging models such as GANs [21, 24, 58], autoregressive [36–38], and diffusion models [6, 51, 64]. Dif-

fusion models, in particular, have demonstrated a strong capacity to iteratively refine images, improving quality with each denoising step to meet specified input constraints, whether text or reference images. Nonetheless, they struggle to maintain consistency in generated images when simulating free camera movement in the scene. For example, [6, 9, 37, 44] generally rely on Monocular Depth Estimation (MDE) [3, 34] and inpainting/outpainting to iteratively expand the scenes. While effective in some scenarios, the success of explicit-based schemes largely depends on the precision of depth estimation models. Consequentially, these methods often struggle with incomplete or noisy depth maps, which can lead to distortions, misaligned details, and inconsistencies in view transition and scene layout [43]. Others [12, 29] train the models to be conditioned on multi-view inputs to better address the challenge. However, these approaches are computationally intensive, as they demand substantial resources to fine-tune such highly complex models. Additionally, fine-tuning could make the models prone to forgetting prior knowledge, limiting their robustness and

practicality [22].

To this extent, we introduce PointmapDiffusion, a novel framework that enables the application of pre-trained 2D diffusion models for NVS by embedding a sense of 3D structure into 2D diffusion features. Central to our approach is the extraction of geometric features and structure details in the form of pointmaps, which represent rasterized 3D coordinates extracted from the scene’s point cloud, alongside diffusion features from reference images. Specifically, to strengthen feature alignment and reinforce the model’s understanding of spatial coherence, we incorporate a Pointmap ControlNet [66]—a neural network structure designed to condition diffusion models by introducing additional trainable copy. By encoding pointmap features, ControlNet enhances the diffusion model’s capacity to capture spatial correspondences between multiple pointmaps, effectively bridging the gap between the reference and target views. This conditioning enables the model to extract relevant geometric relationships for accurate viewpoint transformation. The use of ControlNet eliminates the need for extensive retraining or fine-tuning that state-of-the-art approaches frequently require. Furthermore, PointmapDiffusion employs a reference cross-view attention module that generates novel target views through a denoising diffusion process, guided by the established correspondences between pixels of two pointmaps. This facilitates a seamless flow of geometric and semantic information from the reference view to the generated target view. As a result, we conduct extensive quantitative and qualitative studies on real-world indoor and outdoor datasets to evaluate the proposed approach. Our results demonstrate that the model improves the consistency and the quality of synthesized views with fewer tuned parameters.

To summarize, our main contributions are as follows:

- we propose a pointmap-conditioned generative framework, that can synthesize viewpoints from a single or a variable number of reference views,
- by utilizing reference-view attention to effectively capture correspondences from pointmaps, our method achieves seamless transfer of features from reference views to novel target viewpoints,
- we showcase PointmapDiffusion’s robust performance across indoor and outdoor environments, as well as its effectiveness in both NVS and object manipulation tasks.

## 2. Related Work

**Image & Video Diffusion Models** have achieved state-of-the-art results in unconditional as well as text-guided image generation [11, 16, 31, 39]. Soon after, foundational models such as DALL-E [33], Stable Diffusion [39], and Imagen [41], trained on large-scale datasets, showcase remarkable abilities in creating stunning art within seconds. Since they are primarily trained on single, independent views,

they could not infer the spatial information necessary for accurately rendering scenes from multiple perspectives.

Video diffusion models [5, 15, 17] follow these impressive capabilities in generating realistic videos. While recent video diffusion models are believed to implicitly reason about 3D structures, they still lack the ability to explicitly control the camera viewpoint in the generated videos, making it challenging to leverage off-the-shelf video diffusion models for 3D generation. Despite this limitation, the temporal consistency learned by attention modules presents a valuable asset that can be leveraged to address the challenge of view synthesis [12, 52].

**Novel View Synthesis (NVS).** The goal of NVS is to generate realistic and visually coherent images of a specific instance or scene from camera viewpoints that have not been observed before. This involves taking one or more existing views of the scene and synthesizing new views while ensuring consistency in geometry and appearance. This is particularly important in applications such as virtual reality and 3D reconstruction.

NVS can be categorized into two types based on how viewpoints are generated: *View Interpolation*, where the synthesized viewpoints lie within the given input views distribution, and *View Extrapolation*, which involves generating viewpoints outside the input range, often requiring the model to infer a significant amount of unseen content.

Many modern view interpolation methods are *reconstruction-based* and built upon NeRF [28], 3GDS [19], and their derivatives [50], which describe a scene as radiance fields to fit the observed images. They enable 3D representation by capturing photos of a real scene and optimizing the underlying geometry and appearance. This allows for rendering the scene from any viewpoint in the training poses distribution. However, these methods typically require extensive per-scene fitting and struggle to generate realistic details in unseen regions. Moreover, capturing detailed scenes requires hundreds to thousands of images, and insufficient scene coverage can lead to optimization issues, resulting in inaccurate geometry and blurry renderings when viewed from far-away perspectives.

On the other hand, extrapolation methods are *generative-based* and rely on training generative models to take available reference images and camera viewpoints as conditions, and directly generate new views. These methods are designed to work with minimal initial input (*e.g.* a single image) and rely on leveraging general knowledge from large datasets to plausibly hallucinate unseen content. Pioneer works focus on relatively constrained camera motions around a single object, [26, 42, 57, 70] achieve powerful generalization capability by fine-tuning text-to-image models on object-centric datasets [1, 10, 35]. In contrast, another line of work addresses scenes with arguably

more complex camera trajectories. Especially, ReconFusion [59] and GeNVS [7] uses priors from CLIP image embedding [32] and pixelNeRF’s [63] features for enabling 3D-awareness. Other works [12, 36, 49, 51, 64] designed special attention mechanisms based on epipolar geometry, local neighborhoods, or camera’s ray embeddings [45]. GeoGPT [38], GenWarp [43] and MultiDiff [29] focus on implicit geometric warping signals using MDE [3, 34]. They address challenges related to noisy depth input and viewpoint consistency to enhance scene coherence across generated views. PolyOculus [65] proposes a set-based generative model that can maintain image quality over large sets of images by condition on a variable number of keyframes.

While the mentioned methods require intensive training across large datasets and numerous parameters, our approach is distinct in its efficiency. We design the architecture to focus on tuning only a minimal subset of parameters by leveraging ControlNet [66]. With this, we ensure that the model can adapt to new views and scenes with small adjustments, providing consistent results that maintain alignment with the reference viewpoint. In contrast, our method inspires but also stands out from [2, 30, 61] as we focus on scene-level view synthesis rather than object-level appearance transfer.

### 3. Method

#### 3.1. Preliminaries

**Diffusion Models** [14] are probabilistic models designed to learn the underlying data distribution  $p(x)$  by starting from a Gaussian distributed variable  $x_T$  and gradually denoising it to recover the original data sample  $x_0$ , which simulates the reverse process of a fixed forward (noise-adding) Markov Chain.

In particular, we leverage Latent Diffusion Models (LDM) [39], which utilize a pre-trained Variational Auto-Encoder (VAE) [20] to map image data from pixel space into a compressed latent space with lower dimensionality and performs diffusion process in that latent space. This reduces computational complexity, memory footprint, and enables conditioning on other modalities such as text during generation while still preserving details. Typically, to learn the denoising process, the network, U-Net [40] in this case, is trained to predict the noise by minimizing:

$$\mathcal{L}(\theta) = \mathbb{E}_{\epsilon, \tau} [\|\epsilon - \epsilon_\theta(z_\tau, \tau, \mathbf{c})\|_2^2] \quad (1)$$

where  $\epsilon_\theta$  is the noise prediction network with parameters  $\theta$ ,  $\tau \sim \mathcal{U}(0, T)$  is the time step,  $z_\tau$  is the noisy latent at  $\tau$ ,  $\epsilon \sim \mathcal{N}(0, I)$  is the additive Gaussian noise, and  $\mathbf{c}$  denotes the user-specified conditions, which are used for the conditional generation.

**ControlNet** [66] is a versatile network that allows the addition of conditioning into a pre-trained SD model. It has

been demonstrated to support various types of input conditioning, such as depth, sketches, and semantic maps by injecting conditional image features into trainable copies of the original SD encoder blocks, enabling SD to generate images coherent with the input condition. A key advantage of ControlNet is its ability to resist overfitting during fine-tuning, allowing it to retain the original model’s performance. This makes it particularly useful for incorporating 3D awareness [54, 60] into diffusion models without compromising their 2D semantic quality. Nonetheless, this ability has not yet been fully exploited in view synthesis applications.

**Problem Statement.** Given a reference image  $I^r$  with its depth map  $D^r$ , we aim to generate a novel view  $I^t$  from a relative viewpoint  $P_{r \rightarrow t} \in SE(3)$  and a camera intrinsic  $K \in \mathbb{R}^{3 \times 3}$ . In latent space, our objective becomes:

$$z^t \sim p(z^t | z^r, D^r, P_{r \rightarrow t}, K) \quad (2)$$

where  $z^t, z^r$  are the latent representations for  $I^t, I^r$  and can be decoded through the VAE’s decoder.

#### 3.2. Architecture

Our approach comprises a two-stream architecture, the reference U-Net takes the input view image  $I_r$  and produces a semantic feature  $f_r$  of the input view. Concurrently, the target U-Net takes a noisy latent and generates a novel view image  $I_t$ , by integrating the input view feature  $f_r$  into its internal novel view feature  $f_t$ . To imbue the diffusion model with the depth-based correspondence, we generate a pair of pointmaps  $\{\mathcal{X}^{r,t}, \mathcal{X}^{t,t}\}$  both in the same target coordinate frame and inject them using the two ControlNets. An overview of the architecture of our approach is shown in Fig. 2.

#### 3.3. Pointmap ControlNet.

The advantages of pointmap have been explored in DUST3R [55]. Pointmaps encapsulate the geometry of the scene, the relation between pixels and 3D points, and the relationship between two viewpoints. Such powerful representation can be easily applied to a variety of Multi-View downstream tasks, such as point matching and relative pose estimation. As the potential of pointmaps has not been thoroughly explored, in this work, we further investigate their benefits in the context of diffusion models.

We first revisit the term *pointmap*, a pointmap  $\mathcal{X} \in \mathbb{R}^{W \times H \times 3}$  is a one-to-one mapping between image pixels and 3D scene points. The pointmap  $\mathcal{X}$  of the observed scene can be straightforwardly obtained from the camera intrinsic  $K$  and the ground-truth depth  $D$  as  $\mathcal{X}_{i,j} = K^{-1}D_{i,j}[i, j, 1]^T$ , where each pixel represents the projected point coordinate. Here,  $\mathcal{X}$  is expressed in the camera coordinate frame but in practice, it can further be denoted as

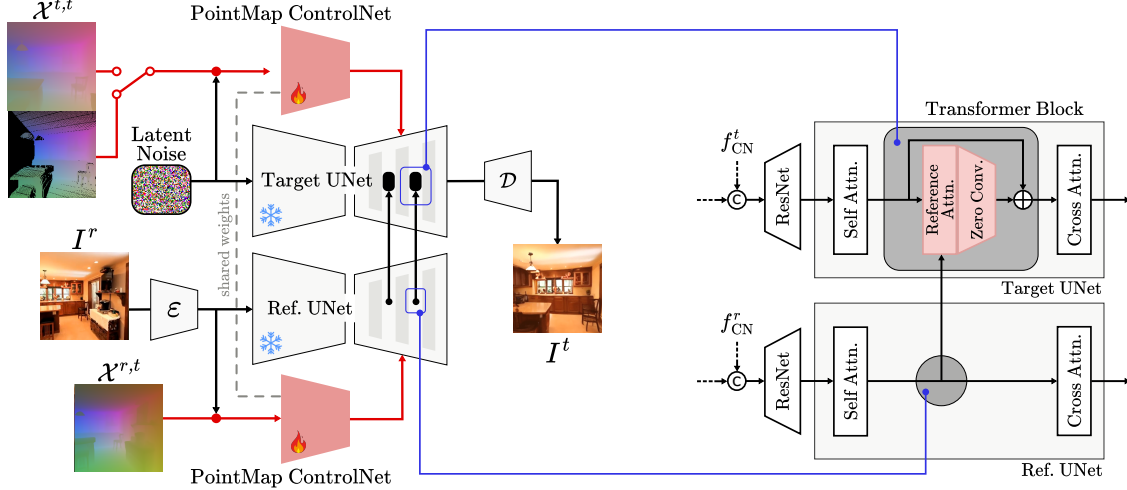


Figure 2. **Method overview.** (left) Our PointmapDiffusion model is trained in the latent space of a fixed VAE with encoder  $\mathcal{E}$  and decoder  $\mathcal{D}$ . Given a reference RGB image  $I^r$  and the corresponding depth  $D^r$ , we obtain a pair of pointmaps  $\{\mathcal{X}^{r,t}, \mathcal{X}^{t,t}\}$  as the input to the model. We predict the target image  $I^t$  given the geometry signal from the target pointmap, and information comes from the reference U-Net. Particularly, two Pointmap ControlNets are employed to extract geometric feature correspondences and concatenate  $\odot$  them with the intermediate SD feature maps. We freeze the original SD model and only train the Pointmap ControlNet and the reference attention module. (right) We extract reference features using our reference U-Net. These augmented features are integrated into the target U-Net through a reference-guided cross-view attention mechanism, which is added  $\oplus$  throughout the mid- and up-block of the target U-Net.

$\mathcal{X}^{n,m}$  which is the pointmap  $\mathcal{X}^n$  from camera  $n$  expressed in camera  $m$ 's coordinate frame:

$$\mathcal{X}^{n,m} = h^{-1}(P_{n \rightarrow m} h(\mathcal{X}^n)) \quad (3)$$

where  $P_{n \rightarrow m}$  is the relative camera poses for images  $m$  and  $n$ , and  $h : (x, y, z) \rightarrow (x, y, z, 1)$  is the homogeneous mapping.

We utilize ControlNet to enhance the 3D awareness of diffusion features by injecting pointmap into the model. Specifically, we select pairs of images with known relative camera poses and train the ControlNet to condition on the two pointmaps  $\{\mathcal{X}^{r,t}, \mathcal{X}^{t,t}\}$ . We suppose  $\mathcal{F}(\cdot; \Theta)$  is an SD block, with parameters  $\Theta$ , in particular, the original ControlNet block copies from pre-trained SD's as  $\mathcal{F}(\cdot; \Theta')$  and accompanies with two zero convolutions  $\mathcal{Z}(\cdot; \Theta_{z1}), \mathcal{Z}(\cdot; \Theta_{z2})$ . Since the geometric features induced by the pointmap condition in ControlNet are designed to be aligned with the latent inputs, they are processed through the zero-initialized convolutions and subsequently added to the spatial layers of the U-Net, as:

$$f_{CN}^m = \underbrace{\mathcal{F}(z; \Theta)}_{\text{semantic feature}} + \underbrace{\mathcal{Z}(\mathcal{F}(z + \mathcal{Z}(\gamma(\mathcal{X}^{m,t}); \Theta_{z1}); \Theta'); \Theta_{z2}))}_{\text{geometric feature}} \quad (4)$$

where  $f_{CN}^m$  with  $m \in \{r, t\}$  is the set of residual signals, which are augmented with the extracted geometric features to join in the features of the middle and upsampling blocks in the diffusion model. The pointmap is then transformed using positional encoding [47] function  $\gamma(\cdot)$ .

We incorporate these two shared-weight ControlNets into the dual U-Net branches to help extract the intermediate feature correspondences between the reference and target pointmaps  $\{\mathcal{X}^{r,t}, \mathcal{X}^{t,t}\}$ . Since both pointmaps are aligned in the same target view coordinate system, the model can naturally follow these geometric correlations between the reference and target views.

### 3.4. Reference-Guided Cross-View Attention.

Our next step is to learn an attention mechanism between the reference and target features, ensuring consistency across different views. We introduce reference-view attention and inject it after the self-attention layer in the main target U-Net, this allows the model to better capture the corresponding relationships from the reference views during the generation process. In this module, we change the keys and values corresponding to the output image  $I^t$  with those of the reference image  $I^r$ . Formally, the output of our reference-view attention layer is given by:

$$\text{RefAttn}(Q^t, K^r, V^r) = \text{softmax} \left( \frac{Q^t K^{rT}}{\sqrt{d}} \right) \cdot V^r$$

$$\text{with } Q^t = W^Q f^t; K^r = W^K f^r; V^r = W^V f^r \quad (5)$$

where  $W^Q, W^K, W^V$  are learnable projection matrices [53] for the feature inputs  $f^r, f^t$ . We further initialize this attention module with the weights from the self-attention module. The output is then passed through a zero



Figure 3. Given a query point in the upper-left generated view and reference views, we extract PointmapDiffusion’s intermediate layer activations through the keys and queries of self-attention and reference attention layers at a certain time step  $\tau = 0.2$  during its backward process and use them to visualize the attention maps [2, 48]. As a result, the method is able to learn and produce correct correspondences.

convolution layer and added back to the information flow.

$$f = f + \mathcal{Z}(\text{RefAttn}(Q^t, K^r, V^r), \Theta_z) \quad (6)$$

We verify the roles of the keys and queries in Fig. 3; they determine the regions in the source view that can be used for generation. Additionally, when leveraging off-the-shelf MDE models [3, 34], the generated depth maps  $D^r$  used for wrapping and establishing point correspondences can be noisy. However, our reference attention mechanism additionally injects both semantic and geometric multi-resolution information from the reference image as a guiding signal. This enables the model to be more robust to noisy depth naturally within the generative prior compared to the warping [6, 9, 37, 44] approach.

### 3.5. Multi-View Conditioned Generation.

Our method can be easily extended to condition on a set of multiple reference images,  $\{I^{r_1}, \dots, I^{r_k}\}$ . This is achieved by concatenating the keys and values from all the reference images, as all pointmaps share the same coordinate system (i.e., the target coordinate). This allows the model to naturally integrate information from multiple reference views, enhancing the quality and consistency of the generated output. Formally, the key and value with multiple images guidance are obtained with the following expressions:

$$K^r = W^K[f^{r_1}, \dots, f^{r_k}]; V^r = W^V[f^{r_1}, \dots, f^{r_k}]. \quad (7)$$

While our model has been trained using only one reference view as a conditioning signal, it is worth to emphasize

that thanks to a careful design, it can benefit from multiple reference view conditioning without further fine-tuning or modification. This allows the model to inherently decide which views it should rely more on during generation.

### 3.6. Training

**Implementation Details.** We define an axis-aligned bounding box (AABB) for the scene based on the two calculated pointmaps to normalize the point values to a fixed range of  $[-1, 1]$ . This normalization reduces the model’s sensitivity to 3D scale ambiguities as we do not explicitly condition on camera poses.

**Training Objective.** We leverage the pre-trained SD v1.5 model for both U-Net branches to inherit its generalization ability. We freeze the VAE, the two U-Nets and train only the reference attention modules with the Pointmap Control-Net by minimizing the following cost function:

$$\mathcal{L}(\theta) = \mathbb{E}_{\epsilon, \tau} [\|\epsilon - \epsilon_\theta(z_\tau^t, z^r, \mathcal{X}^{r,t}, \mathcal{X}^{t,t}, P_{r \rightarrow t}, K, \tau)\|_2^2], \quad (8)$$

on a dataset containing pairs of source view image  $I^r$ , target view image  $I^t$  that are encoded into  $z^r, z^t$  respectively, their camera information  $\{P_{r \rightarrow t}, K\}$ , and pointmaps  $\{\mathcal{X}^{r,t}, \mathcal{X}^{t,t}\}$ . We adopt DDIM sampler [46] during inference.

**Data Augmentation.** During training, having access to the target ground truth depth, we randomly choose between the full target pointmap and the partial target pointmap projected from the reference depth. This approach encourages the model to not only follow the local geometry provided by the pointmap and leverage the semantic information embedded in the reference views but also to robustly infer and complete unobserved regions where no points are available.

## 4. Evaluation

### 4.1. Experimental Setup

**Datasets.** We train and evaluate our model on multiple datasets, including indoor RealEstate10K [69], ScanNet++ [62], and outdoor KITTI-360 [23] datasets. For ScanNet++, we render depth maps from the given scene mesh and the camera information. For RealEstate10K, ground-truth depth maps are not provided, so we pre-process the datasets to generate pseudo-ground-truth depth maps and their corresponding camera information. For KITTI-360, we complete the projected depth [68] obtained from LiDAR data. All images and depth maps are resized and center-cropped to  $256 \times 256$ . We refer to the supplementary material for additional information on data pre-processing.

**Baseline.** Our baseline methods include GeoGPT [38], Photoconsistent-NVS [64], the warping and inpainting method using the SD Inpainting [39], and Gen-

Warp [43]. To ensure fair comparison, we train our model on RealEstate10K, aligning with the training data used by our baselines, and further evaluate on ScanNet++ to assess performance on out-of-distribution scenarios.

**Metrics.** Similar to [36, 43], we consider dividing into short-term and long-term view synthesis. Specifically, we randomly select 1k sequences from the test set with more than 200 frames and evaluate the 50<sup>th</sup> generated frame as short-term and the 100<sup>th</sup> generated frame as long-term view synthesis on RealEstate10K. Due to the faster camera movement in ScanNet++, we focus solely on short-term synthesis, evaluating every 50<sup>th</sup> frame in each sequence. For short-term, we use pairwise reconstruction metrics PSNR, SSIM [56], and LPIPS [67] to measure the difference between the generated and ground-truth images. For long-term, we measure generated image quality, using the FID [13] and KID ( $\times 100$ ) [4] scores to estimate the realism of the generated sequences.

## 4.2. Results

We present two versions of our model, *PointmapDiff*, which is conditioned only on points from the reference depth map, and *PointmapDiff-Full*, which has access to the target depth map. The idea is to see if the model could follow the geometric structure given by the point cloud.

Tab. 1 demonstrates that while GeoGPT gives good FID and KID, indicating realistic generation quality, it struggles with misalignment issues from the input view, leading to lower PSNR and SSIM scores. In contrast, the inpainting-based method excels in PSNR and SSIM, benefiting from explicit warping strategies. However, it often suffers from artifacts due to imperfect warping, resulting in lower FID and KID.

	Short-term			Long-term	
	PSNR $\uparrow$	SSIM $\uparrow$	LPIPS $\downarrow$	FID $\downarrow$	KID $\downarrow$
GeoGPT [38]	14.97	0.424	0.356	<b>28.42</b>	<b>0.158</b>
Photo-NVS [41]	15.74	0.484	0.309	30.96	<u>0.305</u>
Inpainting [39]	<u>16.29</u>	<u>0.568</u>	0.300	47.63	1.546
GenWarp [43]	15.87	0.494	<u>0.237</u>	<u>29.65</u>	0.446
PointmapDiff	16.02	0.500	0.270	38.40	1.183
PointmapDiff-Full	<b>17.52</b>	<b>0.579</b>	<b>0.213</b>	34.54	1.097

Table 1. Quantitative comparisons with SoTA methods on RealEstate10K [69].

For the out-of-distribution experiment, we omit GenWarp as the publicly available model was trained on a similar dataset. As shown in Tab. 2, GeoGPT and Photoconsistent-NVS struggle to generalize to out-of-domain scenarios, resulting in poor performance metrics and a noticeable drop in generation quality. On the other hand, our method achieves stable and consistent results

across both in-domain and out-of-domain datasets, indicating improved adaptability and maintaining high-quality view synthesis under diverse conditions while mitigating overfitting.

	Short-term				
	PSNR $\uparrow$	SSIM $\uparrow$	LPIPS $\downarrow$	FID $\downarrow$	KID $\downarrow$
GeoGPT [38]	14.50	0.520	0.328	62.70	2.256
Photo-NVS [41]	11.72	0.403	0.525	90.05	4.143
Inpainting [39]	15.09	<b>0.630</b>	0.312	56.08	1.647
PointmapDiff	<u>15.19</u>	0.536	<u>0.303</u>	<u>40.16</u>	<u>0.560</u>
PointmapDiff-Full	<b>16.15</b>	<u>0.568</u>	<b>0.248</b>	<b>38.05</b>	<b>0.546</b>

Table 2. Quantitative comparisons with SoTA methods on ScanNet++ [62].

Fig. 4 shows qualitative comparisons on RealEstate10K and ScanNet++. The inpainting model performs well in regions where there is a clear overlap between the input and the novel views. However, in areas with sparse warped pixels, it produces inconsistent novel views, failing to take into account the information from the surrounding input pixels, which impacts the overall coherence. Our method consistently synthesizes realistic and stable novel views across both small and large viewpoint changes, compatible with the quality of GenWarp. Notably, our model achieves these results with significantly reduced parameters being trained, around 50% of a standard U-Net model, compared to 100% for PhotoNVS and 200% for GenWarp. By providing the full target pointmap, PointmapDiff-Full surpasses most of the baselines thanks to its ability to preserve scene structure and transfer appearance plausibly from the input image.

## 4.3. Ablation Study

For this section, we re-train all the variants on the KITTI-360 [23] dataset and we also provide the full target depth to study the conditioning ability of our ControlNet (PointmapDiff-Full). Tab. 3 and Fig. 5 demonstrate the results of our study.

Ablation	LPIPS $\downarrow$	FID $\downarrow$	KID $\downarrow$
w/o Pointmap ControlNet	0.564	39.50	0.936
w/o Ref-Attention	0.608	64.57	3.626
w/o Pointmap P.E.	0.299	24.80	0.276
Full model	<b>0.283</b>	<b>21.26</b>	<b>0.268</b>

Table 3. Ablation of individual components of our pipeline on KITTI-360 [23].

**Pointmap ControlNets.** When excluding the pointmap ControlNets, the model loses access to the correct correspondences derived from the reference image. This omission impairs its ability to maintain spatial consistency, re-

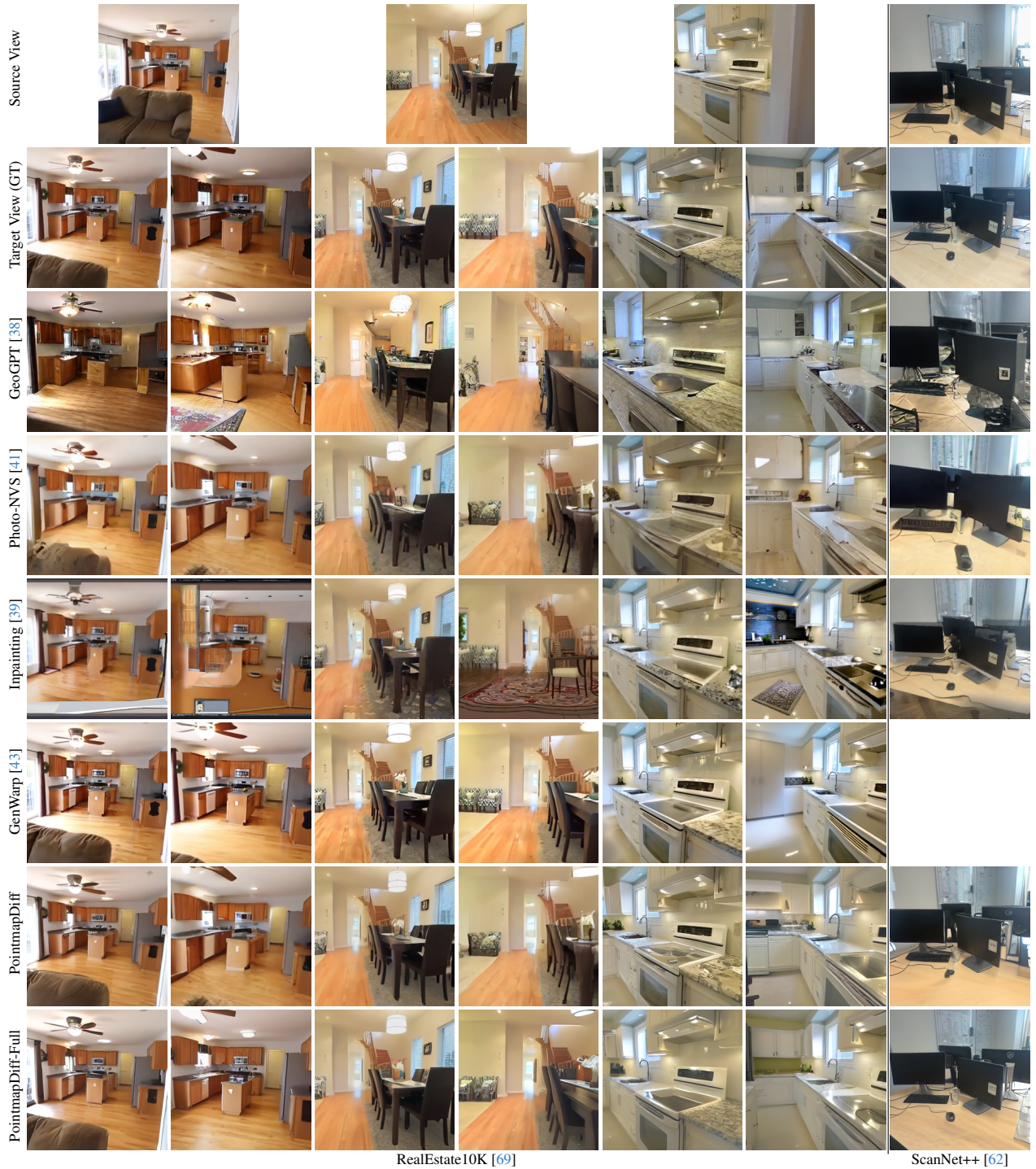


Figure 4. Novel views comparison given a reference view on RealEstate10K [69] and ScanNet++ [62].

sulting in generated views that respect the reference appearance but deviate significantly in geometry (Fig. 5d).

**Reference-Guided Cross-View Attention.** Without reference-view attention, the model operates similarly to a standard geometry-controlled SD model. Even when

we employ LLaVA [25] to input more detailed scene descriptions, the model struggles to respect the reference image. However, this version provides valuable insights—specifically, it demonstrates that pointmaps are an effective conditioning source. They successfully encode the scene’s

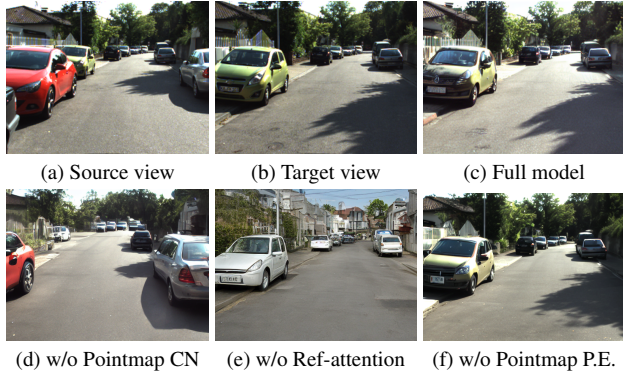


Figure 5. The full model effectively captures high-detail scene continuity, closely aligning with the target image; however, removing components leads to a loss in both geometric structure and fidelity.

geometry, helping the model recover the scene’s structure reasonably, only without precise adherence to the reference image. In Fig. 5e, while the model can place the cars in the correct position, it fails to accurately transfer the appearance from the source image.

**Pointmap Positional Encoding.** Fig. 5f shows that directly passing pointmap coordinates into the network results in reduced image detail (*e.g.* texture on the road and the shadow regions) and lower performance metrics, whereas preprocessing the input with positional embedding (Fig. 5c) enables the model to represent higher frequency details.

**Single-View vs. Multi-View Conditioning.** We use two reference views and compare them with single-view conditions, we use both perspective stereo cameras so that they respect the minimum frame distance for fair comparison. Tab. 4 indicates multi-view conditioning achieves better metrics as it likely solves occlusion problems where one reference viewpoint could not observe several regions within the scene.

	LPIPS↓	FID↓	KID↓
Single-view conditioning	0.283	<b>21.26</b>	0.268
Multi-view conditioning	<b>0.255</b>	23.35	<b>0.235</b>

Table 4. Ablation of multi-view and single-view conditioning on KITTI-360 [23].

#### 4.4. Discussion

In this section, we explore additional capabilities granted by the architecture design of PointmapDiffusion, along with its current limitations.

**Point Modalities Augmentation.** We observe that when doing augmentation, by randomly injecting sparse LiDAR point cloud during training, our model can still generate

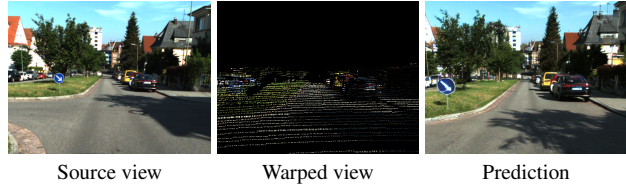


Figure 6. Given very sparse warped results, it’s nearly impossible for the inpainting approach to recover the scene. Nonetheless, our method is able to synthesize target views based on sparse valid pointmaps.

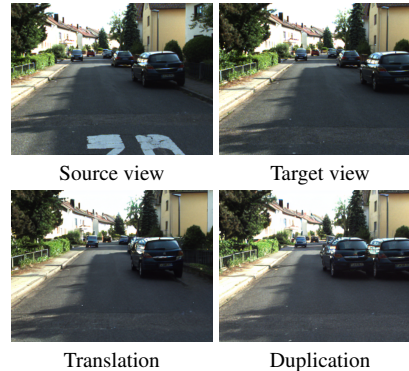


Figure 7. **Scene editing results.** The proposed pipeline achieves instance-level editing by manipulating pointmap values.

high-fidelity views with only 10% of points available, as shown in Fig. 6.

**Objects Manipulation.** Our model allows image editing by manipulating the pointmap, which enables repositioning or duplicating objects within a scene without changing their visual appearances. We first isolate the points belonging to the objects of interest using 3D bounding boxes or instance labels. Then, spatial transformations are applied to these points while preserving their initial values of the pointmap, helping the model to establish correspondences based on these transformations. Following this idea, we showcase in Fig. 7 two scenarios where we shift and duplicate a set of points that belong to a car. As a result, we can perform both novel view synthesis and spatial editing at the same time. This provides a promising direction for future explorations in scene manipulation through pointmap-based editing.

**Limitations.** Our model struggles to adapt effectively when point distributions shift significantly, such as transitioning from indoor to outdoor driving scenes. In such cases, users might need to fine-tune the model for better adaptation. Moreover, despite achieving steerable generation, the current editing process cannot satisfy pixel-level scene control. We hope our method can be a starting point for the large-scale scene editing task, and leave addressing the above issues as future work.



## 5. Conclusion

PointmapDiffusion offers an efficient solution to single-image novel view synthesis by seamlessly combining 2D diffusion models with 3D geometric awareness through pointmap-based conditioning. Unlike traditional methods requiring extensive multi-view data, our method relies on minimal tuning and effectively synthesizes high-quality, consistent views with fewer parameters. Evaluations across real-world datasets confirm its robustness in in-domain and out-of-domain settings, from multiple point modalities, and open new editable view synthesis applications.

## References

- [1] Henrik Aanæs, Rasmus Ramsbøl Jensen, George Vogiatzis, Engin Tola, and Anders Bjarholm Dahl. Large-scale data for multiple-view stereopsis. *International Journal of Computer Vision*, 120:153–168, 2016. [2](#)
- [2] Yuval Alaluf, Daniel Garibi, Or Patashnik, Hadar Averbuch-Elor, and Daniel Cohen-Or. Cross-image attention for zero-shot appearance transfer. In *ACM SIGGRAPH 2024 Conference Papers*, pages 1–12, 2024. [3](#), [5](#)
- [3] Shariq Farooq Bhat, Reiner Birkel, Diana Wofk, Peter Wonka, and Matthias Müller. Zoedepth: Zero-shot transfer by combining relative and metric depth. *arXiv preprint arXiv:2302.12288*, 2023. [1](#), [3](#), [5](#)
- [4] Mikołaj Bińkowski, Danica J Sutherland, Michael Arbel, and Arthur Gretton. Demystifying mmd gans. *arXiv preprint arXiv:1801.01401*, 2018. [6](#)
- [5] Andreas Blattmann, Tim Dockhorn, Sumith Kulal, Daniel Mendelevitch, Maciej Kilian, Dominik Lorenz, Yam Levi, Zion English, Vikram Voleti, Adam Letts, et al. Stable video diffusion: Scaling latent video diffusion models to large datasets. *arXiv preprint arXiv:2311.15127*, 2023. [2](#)
- [6] Shengqu Cai, Eric Ryan Chan, Songyou Peng, Mohamad Shahbazi, Anton Obukhov, Luc Van Gool, and Gordon Wetzstein. Diffdreamer: Towards consistent unsupervised single-view scene extrapolation with conditional diffusion models. In *Proceedings of the IEEE/CVF International Conference on Computer Vision*, pages 2139–2150, 2023. [1](#), [5](#)
- [7] Eric R Chan, Koki Nagano, Matthew A Chan, Alexander W Bergman, Jeong Joon Park, Axel Levy, Miika Aittala, Shalini De Mello, Tero Karras, and Gordon Wetzstein. Generative novel view synthesis with 3d-aware diffusion models. In *Proceedings of the IEEE/CVF International Conference on Computer Vision*, pages 4217–4229, 2023. [3](#)
- [8] Shenchang Eric Chen and Lance Williams. View interpolation for image synthesis. In *Seminal Graphics Papers: Pushing the Boundaries, Volume 2*, pages 423–432. Association for Computing Machinery, 2023. [1](#)
- [9] Jaeyoung Chung, Suyoung Lee, Hyeongjin Nam, Jaerin Lee, and Kyoung Mu Lee. Luciddreamer: Domain-free generation of 3d gaussian splatting scenes. *arXiv preprint arXiv:2311.13384*, 2023. [1](#), [5](#)
- [10] Matt Deitke, Dustin Schwenk, Jordi Salvador, Luca Weihs, Oscar Michel, Eli VanderBilt, Ludwig Schmidt, Kiana Ehsani, Aniruddha Kembhavi, and Ali Farhadi. Objaverse: A universe of annotated 3d objects. In *Proceedings of the IEEE/CVF Conference on Computer Vision and Pattern Recognition*, pages 13142–13153, 2023. [2](#)
- [11] Prafulla Dhariwal and Alexander Nichol. Diffusion models beat gans on image synthesis. *Advances in neural information processing systems*, 34:8780–8794, 2021. [2](#)
- [12] Ruiqi Gao, Aleksander Holynski, Philipp Henzler, Arthur Brussee, Ricardo Martin-Brualla, Pratul Srinivasan, Jonathan T Barron, and Ben Poole. Cat3d: Create anything in 3d with multi-view diffusion models. *arXiv preprint arXiv:2405.10314*, 2024. [1](#), [2](#), [3](#), [12](#)
- [13] Martin Heusel, Hubert Ramsauer, Thomas Unterthiner, Bernhard Nessler, and Sepp Hochreiter. Gans trained by a two time-scale update rule converge to a local nash equilibrium. *Advances in neural information processing systems*, 30, 2017. [6](#)
- [14] Jonathan Ho, Ajay Jain, and Pieter Abbeel. Denoising diffusion probabilistic models. *Advances in neural information processing systems*, 33:6840–6851, 2020. [1](#), [3](#)
- [15] Jonathan Ho, William Chan, Chitwan Saharia, Jay Whang, Ruiqi Gao, Alexey Gritsenko, Diederik P Kingma, Ben Poole, Mohammad Norouzi, David J Fleet, et al. Imagen video: High definition video generation with diffusion models. *arXiv preprint arXiv:2210.02303*, 2022. [2](#)
- [16] Jonathan Ho, Chitwan Saharia, William Chan, David J Fleet, Mohammad Norouzi, and Tim Salimans. Cascaded diffusion models for high fidelity image generation. *Journal of Machine Learning Research*, 23(47):1–33, 2022. [2](#)
- [17] Jonathan Ho, Tim Salimans, Alexey Gritsenko, William Chan, Mohammad Norouzi, and David J Fleet. Video diffusion models. *Advances in Neural Information Processing Systems*, 35:8633–8646, 2022. [2](#)
- [18] Xun Huang and Serge Belongie. Arbitrary style transfer in real-time with adaptive instance normalization. In *Proceedings of the IEEE international conference on computer vision*, pages 1501–1510, 2017. [12](#)
- [19] Bernhard Kerbl, Georgios Kopanas, Thomas Leimkühler, and George Drettakis. 3d gaussian splatting for real-time radiance field rendering. *ACM Trans. Graph.*, 42(4):139–1, 2023. [2](#)
- [20] Diederik P Kingma. Auto-encoding variational bayes. *arXiv preprint arXiv:1312.6114*, 2013. [3](#)
- [21] Jing Yu Koh, Harsh Agrawal, Dhruv Batra, Richard Tucker, Austin Waters, Honglak Lee, Yinfei Yang, Jason Baldridge, and Peter Anderson. Simple and effective synthesis of indoor 3d scenes. In *Proceedings of the AAAI Conference on Artificial Intelligence*, pages 1169–1178, 2023. [1](#)
- [22] Ananya Kumar, Aditi Raghunathan, Robbie Jones, Tengyu Ma, and Percy Liang. Fine-tuning can distort pretrained features and underperform out-of-distribution. *arXiv preprint arXiv:2202.10054*, 2022. [2](#)
- [23] Yiyi Liao, Jun Xie, and Andreas Geiger. Kitti-360: A novel dataset and benchmarks for urban scene understanding in 2d and 3d. *IEEE Transactions on Pattern Analysis and Machine Intelligence*, 45(3):3292–3310, 2022. [5](#), [6](#), [8](#)

- [24] Andrew Liu, Richard Tucker, Varun Jampani, Ameesh Makadia, Noah Snavely, and Angjoo Kanazawa. Infinite nature: Perpetual view generation of natural scenes from a single image. In *Proceedings of the IEEE/CVF International Conference on Computer Vision*, pages 14458–14467, 2021. 1
- [25] Haotian Liu, Chunyuan Li, Yuheng Li, and Yong Jae Lee. Improved baselines with visual instruction tuning. In *Proceedings of the IEEE/CVF Conference on Computer Vision and Pattern Recognition*, pages 26296–26306, 2024. 7
- [26] Ruoshi Liu, Rundi Wu, Basile Van Hoorick, Pavel Tokmakov, Sergey Zakharov, and Carl Vondrick. Zero-1-to-3: Zero-shot one image to 3d object. In *Proceedings of the IEEE/CVF international conference on computer vision*, pages 9298–9309, 2023. 2
- [27] Ben Mildenhall, Pratul P Srinivasan, Rodrigo Ortiz-Cayon, Nima Khademi Kalantari, Ravi Ramamoorthi, Ren Ng, and Abhishek Kar. Local light field fusion: Practical view synthesis with prescriptive sampling guidelines. *ACM Transactions on Graphics (ToG)*, 38(4):1–14, 2019. 1
- [28] Ben Mildenhall, Pratul P Srinivasan, Matthew Tancik, Jonathan T Barron, Ravi Ramamoorthi, and Ren Ng. Nerf: Representing scenes as neural radiance fields for view synthesis. *Communications of the ACM*, 65(1):99–106, 2021. 1, 2
- [29] Norman Müller, Katja Schwarz, Barbara Rössle, Lorenzo Porzi, Samuel Rota Bulò, Matthias Nießner, and Peter Kotschieder. Multidiff: Consistent novel view synthesis from a single image. In *Proceedings of the IEEE/CVF Conference on Computer Vision and Pattern Recognition*, pages 10258–10268, 2024. 1, 3
- [30] Ivona Najdenkoska, Animesh Sinha, Abhimanyu Dubey, Dhruv Mahajan, Vignesh Ramanathan, and Filip Radenovic. Context diffusion: In-context aware image generation. In *European Conference on Computer Vision*, pages 375–391. Springer, 2024. 3
- [31] Dustin Podell, Zion English, Kyle Lacey, Andreas Blattmann, Tim Dockhorn, Jonas Müller, Joe Penna, and Robin Rombach. Sdxl: Improving latent diffusion models for high-resolution image synthesis. *arXiv preprint arXiv:2307.01952*, 2023. 2
- [32] Alec Radford, Jong Wook Kim, Chris Hallacy, Aditya Ramesh, Gabriel Goh, Sandhini Agarwal, Girish Sastry, Amanda Askell, Pamela Mishkin, Jack Clark, et al. Learning transferable visual models from natural language supervision. In *International conference on machine learning*, pages 8748–8763. PMLR, 2021. 3
- [33] Aditya Ramesh, Mikhail Pavlov, Gabriel Goh, Scott Gray, Chelsea Voss, Alec Radford, Mark Chen, and Ilya Sutskever. Zero-shot text-to-image generation. In *International conference on machine learning*, pages 8821–8831. Pmlr, 2021. 2
- [34] René Ranftl, Katrin Lasinger, David Hafner, Konrad Schindler, and Vladlen Koltun. Towards robust monocular depth estimation: Mixing datasets for zero-shot cross-dataset transfer. *IEEE transactions on pattern analysis and machine intelligence*, 44(3):1623–1637, 2020. 1, 3, 5
- [35] Jeremy Reizenstein, Roman Shapovalov, Philipp Henzler, Luca Sbordone, Patrick Labatut, and David Novotny. Common objects in 3d: Large-scale learning and evaluation of real-life 3d category reconstruction. In *Proceedings of the IEEE/CVF international conference on computer vision*, pages 10901–10911, 2021. 2
- [36] Xuanchi Ren and Xiaolong Wang. Look outside the room: Synthesizing a consistent long-term 3d scene video from a single image. In *Proceedings of the IEEE/CVF Conference on Computer Vision and Pattern Recognition*, pages 3563–3573, 2022. 1, 3, 6
- [37] Chris Rockwell, David F Fouhey, and Justin Johnson. Pixel-synth: Generating a 3d-consistent experience from a single image. In *Proceedings of the IEEE/CVF International Conference on Computer Vision*, pages 14104–14113, 2021. 1, 5
- [38] Robin Rombach, Patrick Esser, and Björn Ommer. Geometry-free view synthesis: Transformers and no 3d priors. In *Proceedings of the IEEE/CVF International Conference on Computer Vision*, pages 14356–14366, 2021. 1, 3, 5, 6, 7, 13
- [39] Robin Rombach, Andreas Blattmann, Dominik Lorenz, Patrick Esser, and Björn Ommer. High-resolution image synthesis with latent diffusion models. In *Proceedings of the IEEE/CVF conference on computer vision and pattern recognition*, pages 10684–10695, 2022. 2, 3, 5, 6, 7, 13
- [40] Olaf Ronneberger, Philipp Fischer, and Thomas Brox. U-net: Convolutional networks for biomedical image segmentation. In *Medical image computing and computer-assisted intervention—MICCAI 2015: 18th international conference, Munich, Germany, October 5–9, 2015, proceedings, part III 18*, pages 234–241. Springer, 2015. 3
- [41] Chitwan Saharia, William Chan, Saurabh Saxena, Lala Li, Jay Whang, Emily L Denton, Kamyar Ghasemipour, Raphael Gontijo Lopes, Burcu Karagol Ayan, Tim Salimans, et al. Photorealistic text-to-image diffusion models with deep language understanding. *Advances in neural information processing systems*, 35:36479–36494, 2022. 2, 6, 7, 13
- [42] Kyle Sargent, Zizhang Li, Tanmay Shah, Charles Herrmann, Hong-Xing Yu, Yunzhi Zhang, Eric Ryan Chan, Dmitry Lagun, Li Fei-Fei, Deqing Sun, et al. Zeronvs: Zero-shot 360-degree view synthesis from a single image. In *Proceedings of the IEEE/CVF Conference on Computer Vision and Pattern Recognition*, pages 9420–9429, 2024. 2
- [43] Junyoung Seo, Kazumi Fukuda, Takashi Shibuya, Takuya Narihira, Naoki Murata, Shoukang Hu, Chieh-Hsin Lai, Seungryong Kim, and Yuki Mitsufuji. Genwarp: Single image to novel views with semantic-preserving generative warping. *arXiv preprint arXiv:2405.17251*, 2024. 1, 3, 6, 7, 12, 13
- [44] Jaidev Shriram, Alex Trevithick, Lingjie Liu, and Ravi Ramamoorthi. Realmdreamer: Text-driven 3d scene generation with inpainting and depth diffusion. *arXiv preprint arXiv:2404.07199*, 2024. 1, 5
- [45] Vincent Sitzmann, Semon Rezchikov, Bill Freeman, Josh Tenenbaum, and Fredo Durand. Light field networks: Neural scene representations with single-evaluation rendering. *Advances in Neural Information Processing Systems*, 34:19313–19325, 2021. 3
- [46] Jiaming Song, Chenlin Meng, and Stefano Ermon.

- Denoising diffusion implicit models. *arXiv preprint arXiv:2010.02502*, 2020. 5
- [47] Matthew Tancik, Pratul Srinivasan, Ben Mildenhall, Sara Fridovich-Keil, Nithin Raghavan, Utkarsh Singhal, Ravi Ramamoorthi, Jonathan Barron, and Ren Ng. Fourier features let networks learn high frequency functions in low dimensional domains. *Advances in neural information processing systems*, 33:7537–7547, 2020. 4
- [48] Luming Tang, Menglin Jia, Qianqian Wang, Cheng Perng Phoo, and Bharath Hariharan. Emergent correspondence from image diffusion. *Advances in Neural Information Processing Systems*, 36:1363–1389, 2023. 5
- [49] Shitao Tang, Fuyang Zhang, Jiacheng Chen, Peng Wang, and Yasutaka Furukawa. Mvdifffusion: Enabling holistic multi-view image generation with correspondence-aware diffusion. *arXiv preprint arXiv:2307.01097*, 2023. 3
- [50] Ayush Tewari, Justus Thies, Ben Mildenhall, Pratul Srinivasan, Edgar Tretschk, Wang Yifan, Christoph Lassner, Vincent Sitzmann, Ricardo Martin-Brualla, Stephen Lombardi, et al. Advances in neural rendering. In *Computer Graphics Forum*, pages 703–735. Wiley Online Library, 2022. 2
- [51] Hung-Yu Tseng, Qinbo Li, Changil Kim, Suhil Alsisan, Jia-Bin Huang, and Johannes Kopf. Consistent view synthesis with pose-guided diffusion models. In *Proceedings of the IEEE/CVF Conference on Computer Vision and Pattern Recognition*, pages 16773–16783, 2023. 1, 3
- [52] Basile Van Hoorick, Rundi Wu, Ege Ozguroglu, Kyle Sargent, Ruoshi Liu, Pavel Tokmakov, Achal Dave, Changxi Zheng, and Carl Vondrick. Generative camera dolly: Extreme monocular dynamic novel view synthesis. *arXiv preprint arXiv:2405.14868*, 2024. 2
- [53] Ashish Vaswani. Attention is all you need. *arXiv preprint arXiv:1706.03762*, 2017. 4
- [54] Haiping Wang, Yuan Liu, Bing Wang, Yujing Sun, Zhen Dong, Wenping Wang, and Bisheng Yang. Freereg: Image-to-point cloud registration leveraging pretrained diffusion models and monocular depth estimators. *arXiv preprint arXiv:2310.03420*, 2023. 3
- [55] Shuzhe Wang, Vincent Leroy, Yohann Cabon, Boris Chidlovskii, and Jerome Revaud. Dust3r: Geometric 3d vision made easy. In *Proceedings of the IEEE/CVF Conference on Computer Vision and Pattern Recognition*, pages 20697–20709, 2024. 3, 12
- [56] Zhou Wang, Alan C Bovik, Hamid R Sheikh, and Eero P Simoncelli. Image quality assessment: from error visibility to structural similarity. *IEEE transactions on image processing*, 13(4):600–612, 2004. 6
- [57] Daniel Watson, William Chan, Ricardo Martin-Brualla, Jonathan Ho, Andrea Tagliasacchi, and Mohammad Norouzi. Novel view synthesis with diffusion models. *arXiv preprint arXiv:2210.04628*, 2022. 2
- [58] Olivia Wiles, Georgia Gkioxari, Richard Szeliski, and Justin Johnson. Synsin: End-to-end view synthesis from a single image. In *Proceedings of the IEEE/CVF conference on computer vision and pattern recognition*, pages 7467–7477, 2020. 1
- [59] Rundi Wu, Ben Mildenhall, Philipp Henzler, Keunhong Park, Ruiqi Gao, Daniel Watson, Pratul P Srinivasan, Dor Verbin, Jonathan T Barron, Ben Poole, et al. Reconfusion: 3d reconstruction with diffusion priors. In *Proceedings of the IEEE/CVF Conference on Computer Vision and Pattern Recognition*, pages 21551–21561, 2024. 3
- [60] Chenfeng Xu, Huan Ling, Sanja Fidler, and Or Litany. 3diff-tecton: 3d object detection with geometry-aware diffusion features. In *Proceedings of the IEEE/CVF Conference on Computer Vision and Pattern Recognition*, pages 10617–10627, 2024. 3
- [61] Xingqian Xu, Jiayi Guo, Zhangyang Wang, Gao Huang, Irfan Essa, and Humphrey Shi. Prompt-free diffusion: Taking” text” out of text-to-image diffusion models. In *Proceedings of the IEEE/CVF Conference on Computer Vision and Pattern Recognition*, pages 8682–8692, 2024. 3
- [62] Chandan Yeshwanth, Yueh-Cheng Liu, Matthias Nießner, and Angela Dai. Scannet++: A high-fidelity dataset of 3d indoor scenes. In *Proceedings of the IEEE/CVF International Conference on Computer Vision*, pages 12–22, 2023. 5, 6, 7, 13
- [63] Alex Yu, Vickie Ye, Matthew Tancik, and Angjoo Kanazawa. pixelnerf: Neural radiance fields from one or few images. In *Proceedings of the IEEE/CVF conference on computer vision and pattern recognition*, pages 4578–4587, 2021. 3
- [64] Jason J Yu, Fereshteh Forghani, Konstantinos G Derpanis, and Marcus A Brubaker. Long-term photometric consistent novel view synthesis with diffusion models. In *Proceedings of the IEEE/CVF International Conference on Computer Vision*, pages 7094–7104, 2023. 1, 3, 5
- [65] Jason J Yu, Tristan Aumentado-Armstrong, Fereshteh Forghani, Konstantinos G Derpanis, and Marcus A Brubaker. Polyoculus: Simultaneous multi-view image-based novel view synthesis. *arXiv preprint arXiv:2402.17986*, 2024. 3
- [66] Lvmin Zhang, Anyi Rao, and Maneesh Agrawala. Adding conditional control to text-to-image diffusion models. In *Proceedings of the IEEE/CVF International Conference on Computer Vision*, pages 3836–3847, 2023. 2, 3
- [67] Richard Zhang, Phillip Isola, Alexei A Efros, Eli Shechtman, and Oliver Wang. The unreasonable effectiveness of deep features as a perceptual metric. In *Proceedings of the IEEE conference on computer vision and pattern recognition*, pages 586–595, 2018. 6
- [68] Youmin Zhang, Xianda Guo, Matteo Poggi, Zheng Zhu, Guan Huang, and Stefano Mattoccia. Completionformer: Depth completion with convolutions and vision transformers. In *Proceedings of the IEEE/CVF conference on computer vision and pattern recognition*, pages 18527–18536, 2023. 5
- [69] Tinghui Zhou, Richard Tucker, John Flynn, Graham Fyffe, and Noah Snavely. Stereo magnification: Learning view synthesis using multiplane images. *arXiv preprint arXiv:1805.09817*, 2018. 5, 6, 7, 13
- [70] Zhizhuo Zhou and Shubham Tulsiani. Sparsefusion: Distilling view-conditioned diffusion for 3d reconstruction. In *Proceedings of the IEEE/CVF Conference on Computer Vision and Pattern Recognition*, pages 12588–12597, 2023. 2

# Pointmap-Conditioned Diffusion for Consistent Novel View Synthesis

## Supplementary Material

### A. Implementation Details

#### A.1. PointmapDiffusion Motivation

We further explain the motivation for using pointmaps as conditioning signals. Establishing correspondences  $\mathcal{M}^{r,t}$  between pixels of two images can be trivially achieved by nearest neighbor (NN) search in the 3D pointmap space:

$$\mathcal{M}^{r,t} = \{(a, b) \mid a = \text{NN}^{t,r}(b) \text{ and } b = \text{NN}^{r,t}(a)\} \\ \text{with } \text{NN}^{m,n}(a) = \arg \min_{b \in \{0, \dots, WH\}} \|\mathcal{X}_b^{n,n} - \mathcal{X}_a^{m,n}\|. \quad (9)$$

Here,  $\text{NN}^{m,n}$  computes the nearest neighbor  $b$  of pixel  $a$  between views  $m$  and  $n$ . While this explicit correspondence is computationally expensive and only operates on pixel space, it motivates our approach of leveraging implicit attention mechanisms.

We consider a simple positional encoding example of pointmaps,  $\gamma(\mathcal{X})$ , which maps the normalized input points to higher dimensional Fourier features using a set of sine and cosine functions:

$$\gamma(\mathbf{x}) = [a_1 \cos(2\pi F_1 \mathbf{x}), a_1 \sin(2\pi F_1 \mathbf{x}), \dots, \\ a_N \cos(2\pi F_N \mathbf{x}), a_N \sin(2\pi F_N \mathbf{x})]^T, \quad (10)$$

where  $F_j$  are the Fourier basis frequencies and  $a_j$  are their corresponding coefficients. Using this encoding, the spatial correlation between two pointmaps can be measured via a kernel function as:

$$\gamma(\mathbf{x}_1)\gamma(\mathbf{x}_2)^T = \sum_{j=1}^N a_j^2 \cos(2\pi F_j(\mathbf{x}_1 - \mathbf{x}_2)) \quad (11)$$

To adapt this to the nearest neighbor computation, we redefine  $\text{NN}^{m,n}$  using the encoded pointmaps as follows:

$$\text{NN}^{m,n}(a) = \arg \max_{b \in \{0, \dots, WH\}} \left( \gamma(\mathcal{X}_b^{n,n}) \gamma(\mathcal{X}_a^{m,n})^T \right), \quad (12)$$

replacing  $t \leftarrow n$  and  $r \leftarrow m$ , and applying this for all  $a \in \{0, \dots, WH\}$ , interestingly, this operation resembles the reference attention mechanism introduced in the main paper. Specifically, the attention matrix:  $A = \text{softmax} \left( \frac{Q^t K^{rT}}{\sqrt{d}} \right)$  serves a similar purpose by learning implicit correspondences between the query ( $Q^t$ ) and key ( $K^r$ ) representations extracted from Pointmap ControlNet layers of the target and reference views. Thus, the pointmap conditioning acts as an intermediate signal to naturally establish correspondences within the attention layers, bridging the gap between explicit point matching and feature-based reasoning with the ability to dynamically attend to relevant regions.

#### A.2. Data Processing

We use the same DUST3R [55] model to generate pointmaps for training and as a depth estimator for all baseline methods during inference. Furthermore, we use a small-resolution voxel grid to measure the overlap ratio between the two pointmaps thus choosing the correct image pairs in the test set, *i.e.* all pairs will have overlapping areas between 10% and 90%. The generated pointmap then undergoes a normalization process followed by a positional encoding step.

#### A.3. Model & Training

Our method employs a pre-trained SDv1.5 as the backbone for its robust generative capabilities. Since SDv1.5 is also a text-to-image model, we incorporate simple text prompts, such as "a photo of a room" or "a photo of an office," to provide high-level semantic guidance and enhance the generative process. Unlike other methods [12, 43], we do not modify the latent input, allowing us to retain the U-Net backbone and instead adapt to the task by training the additional ControlNet. Notably, features from the ControlNet are integrated only into the decoder of the U-Net, so we do not need to apply reference attention to the encoder part.

As we notice a color shift between the output and the reference images, we apply AdaIN [18] to the output image. Specifically, we normalize the prediction by subtracting its per-channel mean and dividing by its standard deviation, then introduce the mean and standard deviation from the warped image to align with the color distribution of the reference view.

For the positional encoding, we use a frequency range from  $2^0$  to  $2^3$ , resulting in an input channel dimension of 24 for the ControlNet model. During training, we use a batch size of 4 and train the model for 500k iterations with a learning rate of  $10^{-4}$  and a cosine scheduler. Other training parameters remain set to their default values.

#### A.4. Baseline Details

We use the official checkpoint for all baselines: GeoGPT, Photoconsistent-NVS, SD-Inpainting, and GenWarp. For GeoGPT, we use the `reimpl-depth` model. Moreover, we apply interpolation on the warped results for SD-Inpainting and dilate the inpaint mask using a  $9 \times 9$  kernel to reduce artifacts since the model performs inpainting on latent space. Finally, all outputs are resized and cropped to  $256 \times 256$  for evaluation.

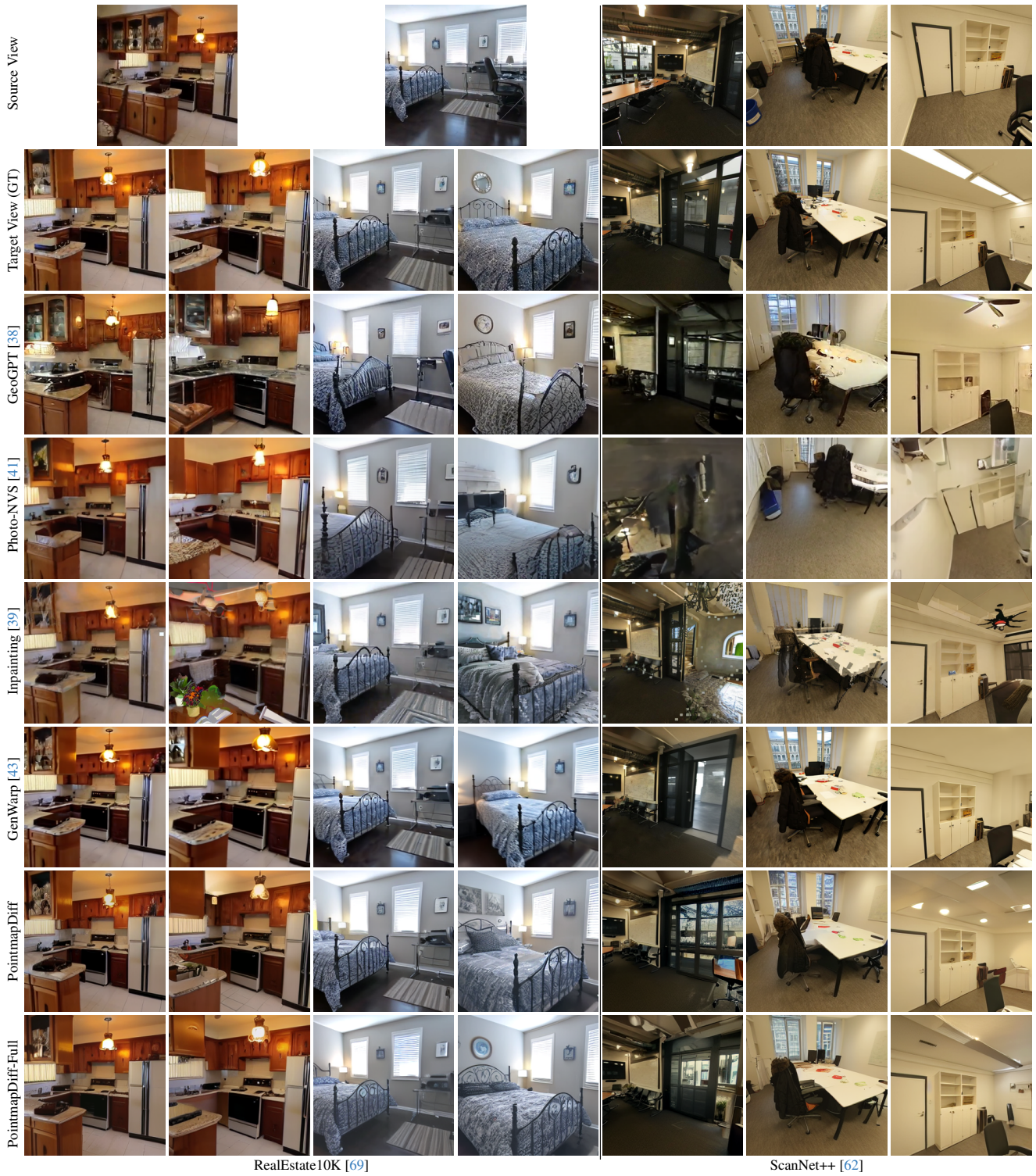


Figure 8. Additional NVS comparison on RealEstate10K [69] and ScanNet++ [62].

## B. Additional Results

Fig. 8 provides additional qualitative comparison. We observe that GeoGPT and Photoconsistent-NVS give worse

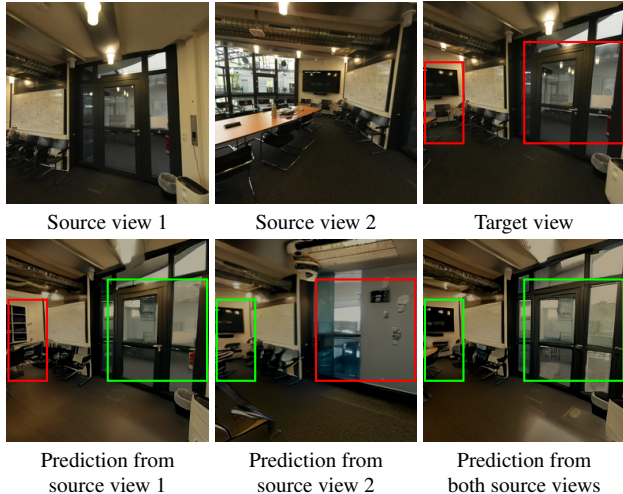


Figure 9. We demonstrate the ability to generate viewpoints situated between two source views, effectively covering occluded regions by combining complementary information from both views. We use **red** to denote hallucinated regions and **green** to indicate aligned regions compared to the target view.

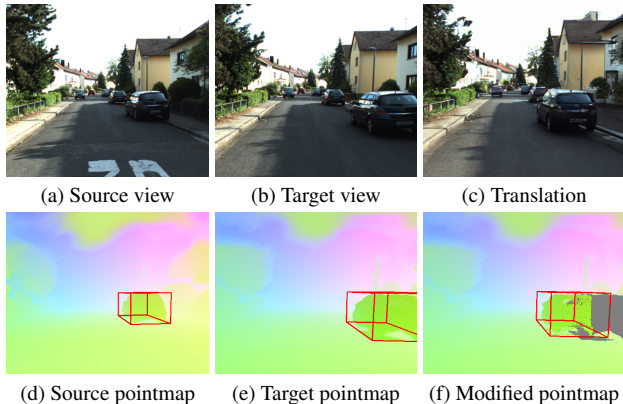


Figure 10. **Translation procedure in pointmap space.** From a structure pointmap of the scene (d), one can move the camera around (e) and relocate the object position (f) while still retaining point correspondences. The transparency of background pixels is increased to ease visualization.

performance in out-of-distribution scenarios. Additionally, when the camera is far away from the reference view, GenWarp tends to prioritize preserving semantic information over geometric consistency.

## C. Additional Analysis

### C.1. Multi-View Conditioning

Our method enables few-shot NVS by conditioning on multi-view inputs, which other baselines cannot do. This technique leverages information from multiple viewpoints, effectively addressing scenarios where certain regions are vis-

ible in one viewpoint but occluded in another and vice versa, ensuring more consistent scene reconstruction as shown in Fig. 9.

### C.2. Pointmap-based Editing

According to Fig. 10, we detail the pointmap modification as follows: given a bounding box of an object of interest (shown in red), we separate the points that lie within the bounding box and apply a transformation on the points. After we have the modified point cloud, to obtain the conditioning signal for scene manipulation, we rasterize the modified point cloud while keeping the old point coordinates as the pixel values. This ensures the object’s shape remains consistent after spatial adjustments and appearance can be transferred correctly. Additionally, we use a z-buffer to handle point occlusions and empty regions that may appear after the transformation will be inpainted during the generation process.